"Practical Surface Analysis," J. Wiley and Sons, London (1983).
27. M. P. Seah and W. A. Dench, *Surf. Int. Anal.*, **1**, 2 (1979); J. C. Ashley and C. J. Tung, *ibid.*, **4**, 52 (1982); C. R. Boundle, *J. Vac. Sci. Technol.*, **11**, 212 (1974).
28. C. D. Wagner, D. E. Passoja, H. F. Hillery, T. G. Kinisky, H. A. Six, W. T. Jansen, and J. A. Taylor, *J. Vac. Sci. Technol.*, **21**, 933 (1982).
29. G. Hollinger, Y. Jugner, P. Pertosa, and Tran Minh Duc, *Chem. Phys. Lett.*, **36**, 441 (1975).
30. J. H. Thomas III, in "Applied ESCA," H. Windawi and P. Ho, Editors, Wiley Interscience, New York (1983).
31. H. E. Bennett and J. O. Porteus, *J. Opt. Soc. Am.*, **51**, 123 (1961).

Structure and Crystallization of Nickel-Phosphorus Alloys Prepared by High-Rate Electrodeposition

Patrick K. Ng,* Dexter D. Snyder,* and Joseph LaSala

General Motors Research Laboratories, Physical Chemistry Department, Warren, Michigan 48090-9055

Bruce Clemens and Carlton Fuerst

General Motors Research Laboratories, Physics Department, Warren, Michigan 48090-9055

ABSTRACT

Thin film nickel-phosphorus alloys are electrodeposited at a high rate using a specialized rapid electrolyte flow system. Current densities up to 2.33 A/cm^2, which are difficult to maintain in conventional plating processes, can be used to produce satisfactory films. The deposits are characterized by x-ray diffraction and differential scanning calorimetry. Phosphorus content decreases with increasing current density and is virtually independent of the electrolyte flow rate above 5.7 m/s, where the system is operating in the turbulent regime. Deposit structure depends strongly on the phosphorus content; it is amorphous or highly microcrystalline at >14 atom percent (a/o) and crystalline at <14 a/o. The low phosphorus deposits decompose directly from a solid solution of nickel and phosphorus to a mixture of nickel and nickel phosphide (Ni_3P) at a temperature in the range of 380°-420°C. The high phosphorus deposits transform first to a metastable intermediate (Ni_xP_y) which subsequently transforms to nickel and nickel phosphide at higher temperatures.

Nickel-phosphorus alloys are of great importance for corrosion protection, wear coating, electrical applications, and catalysis. In the automotive industry, this material is a key layer in the coating of plastic parts for decorative purposes. Nickel-phosphorus coatings have been used successfully in fuel tanks which must resist corrosion from alcohol or alcohol-gasoline mixtures. This coating is further used as a wear resistant layer on tooling, where the inclusion of phosphorus gives a deposit considerably harder than pure nickel (1). Nickel-phosphorus has also been tried for discrete thin film resistors (2). Recently, the catalytic activity of nickel-phosphorus alloys has been reported (3, 4). The large number of recent publications on nickel-phosphorus alloys shows a resurgence of interest in the material and suggests it will be used more widely in the future.

Nickel-phosphorus alloys are facile transition metal-metalloid glass formers which can be created by vacuum deposition, chemical reduction (electroless deposition), rapid quenching, and electrodeposition. Of the two chemical approaches, electroless deposition is the slower, but it has the advantage of uniform surface coverage. A reducing agent here converts the nickel ions to metal, generating included elemental phosphorus. By contrast, electrodeposition is faster, but it cannot cover arbitrary shapes uniformly. This process is field-driven and the surface coverage is thus controlled by electrolyte conductivity and workpiece (cathode) contour.

While electroless deposition is the dominant commercial route for making nickel-phosphorus, there is renewed interest in electroplating the alloy, to gain thicker coatings and higher production rates (5). Electrolytic nickel-phosphorus technology traces back to pioneering work by Brenner at the National Bureau of Standards (6). The electrolytes are typically combinations of nickel sulfate and chloride with phosphoric and phosphorus acids or salts. Mayer *et al.* (7) built up 1 cm spheres from a mixed sulfate-chloride bath at 10 A/dm^2 to demonstrate that amorphous nickel-phosphorus can be electroformed into bulk shapes. Rajagopal (8) also electrodeposited nickel-phosphorus from a similar bath at current densities of 5-15 A/dm^2, reaching thicknesses of about 100 μm. Ratzker *et al.* provided fresh insight on the character of this electrodeposited alloy, using deposits laid down at current densities reaching 150 A/dm^2 (9).

As-plated, the nickel-phosphorus alloy is metastable and highly microcrystalline, even amorphous under certain conditions (10). Nickel-phosphorus is a relatively complex system (Fig. 1) which can form a number of stable compounds (11). Reported electrolytic and electroless deposits contain typically less than 25 atom percent (a/o) phosphorus, and they convert with heating, making the material harder and more brittle (12). As deposited, this material is a supersaturated solution of phosphorus in the face-centered cubic lattice of crystalline nickel. Calorimetry shows a transition around 300°C, the enthalpy of which is proportional to the percent contained phosphorus (13). Two careful studies (12, 14) of the recrystallization of amorphous nickel-phosphorus alloy indicate that below the crystallization temperature, nickel crystals precipitate to a relatively small extent. At the crystallization temperature, crystals of Ni_3P grow at the expense of the fcc Ni phase. The crystallization temperature of under-eutectic alloys also decreases as the phosphorus content rises. Some investigators (12, 15, 16) also found an intermediate phase of Ni_xP_y whose x-ray pattern cannot be indexed.

A complete understanding of the nucleation and film growth in high rate electrodeposition is still lacking. In a simplified view, for a single depositing element, we compute the continuum growth rate for a uniform film as follows

$$\frac{dh}{dt} = \frac{iM}{n\mathbf{F}\rho} \qquad [1]$$

where h is the electrodeposit thickness, M, the molecular weight of metal, n, equivalents per mole, ρ, the metal's density, and $\mathbf{F}$, the Faraday.

For current densities in the range 1-10 A/cm^2, we predict rates to be on the order of 500-5000 nm/s. This implies that

* Electrochemical Society Active Member.

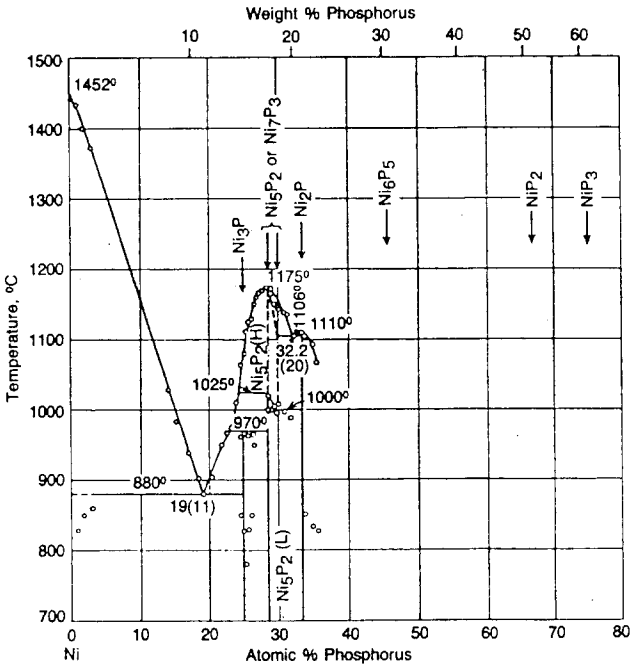

Fig. 1. Phase diagram of Ni-P system [Ref. (22)]

near-neighbors are put in place on a time frame of 10^{-3} to 10^{-4}s.

Since electrodeposition yields metastable nickel-phosphorus films of technological importance, it becomes important for applications to determine how their structure relates to formation conditions. The strategy here was first to identify those metastable structures which form at the high deposition rates now routinely achievable, and next to determine the limiting rate and uniformity with which these thin film structures can be deposited.

Experimental

The high-speed deposition system.—An air pressure driven laboratory deposition system was used to create nickel-phosphorus alloys (18). The solution is driven from one reservoir, with compressed air, through the deposition channel to a second receiver tank. When this second tank is filled, the direction of pumping is reversed. All inner surfaces contacting the solution are lined with inert fluorocarbon material. The electrolyte is maintained at operating temperature by steam heat.

The flow channel fixture is constructed of two Lucite members, clamped and sealed with an O ring. A nickel anode is mounted in the lower section, and a removable copper cathode is inserted in the upper section, held by a set screw. Initial anode-cathode separation is 0.21 cm.

Conditions.—The electrodeposition solution is formulated and run as follows, 150 g/l $NiSO_4 \cdot 6H_2O$; 45 g/l $NiCl_2 \cdot 6H_2O$; 40 g/l H_3PO_3; 49 g/l H_3PO_4; pH 1.0, adjusted with $NiCO_3$ and H_2SO_4; and T 75°C (±2°C).

Copper samples (6.45 cm^2) for the high speed plating are first prepared by the following procedure: 30s ultrasonic clean, 1 min cathodic alkaline clean, water rinse, 30s HCl acid dip, and water rinse and air dry.

Flow rates used were 5.7, 8.7, 11.7, and 14.2 m/s, corresponding to applied air pressures of 10, 20, 30 and 40 psi. Run time and current are adjusted to yield a total plating charge of 1000C. Samples were run in triplicate for each set of conditions.

The electroless bath has a pH of 4.7 and contains $NiCl_2 \cdot 6H_2O$ (30 g/l), $NaH_2PO_2 \cdot 2H_2O$ (10 g/l), and $HOCH_2COOH$ (35 g/l); total plating time was 1h. In the conventional (tank) plating process, the electrolyte used with the high flow system was employed with a moderate agitation provided by a stirrer.

Characterization procedure.—Copper cathodes are weighed before and after deposition to permit current efficiency determination. Deposit morphology and composition are then recorded with scanning electron microscopy and energy dispersive x-ray analysis. As a check, a portion of each film is dissolved in nitric acid and the relative amounts of nickel and phosphorus are determined using atomic absorption spectrometry. The samples are next cut close to the deposit with a slow speed saw, and the copper is removed by soaking the cut portion in chromic acid to make free standing foils for calorimetry and structure analysis. The phase transformations of these metastable foils are studied using differential scanning calorimetry at a heating rate of 50°C/min. X-ray diffractograms are recorded for samples both as-deposited and following various levels of heating. For the as-plated samples, the microstructures were investigated using x-ray diffraction with Seeman-Bohlin thin film geometry. This diffraction geometry utilizes a small fixed incident angle to increase the scattering from a thin film surface region.

Results and Discussion

Effect of plating conditions on composition.—The deposit compositions obtained at different current densities and electrolyte flow rates are summarized in Table I; for comparison, results from both electroless and conventional plating processes are included. Compositions from EDAX measurements agree well with those determined by chemical analyses (Table II). Impurities included low levels (<1.5 a/o) of copper, iron, and cobalt. The current efficiency was calculated according to the following cathodic reaction mechanism

$$Ni^{+2} + 2e^- \rightarrow Ni(s) \quad [2]$$

$$HPO_3^{-2} + 2H_2O + 2e^- \rightarrow H_2PO_2^- + 3\ OH^- \quad [3]$$

Table I. Experimental results

Plating system	Current density (A/cm^2)	Flow rate (m/s)	Composition (a/o) Ni	Composition (a/o) P	Current efficiency (%)	Thickness (μm) Theoretical	Thickness (μm) Measured	Deposition rate (μm/min)
Electroless	—	—	81.6	18.4	—	20.7	20.3	0.33
Conventional plating	0.022	Stirrer	71.0	29.0	29.2	20.0	—	0.17
	0.044	Stirrer	71.2	28.8	24.6	16.8	15.2	0.28
	0.31	5.7	71.3	28.7	18.1	12.3	12.7	1.48
	0.62	5.7	71.6	28.3	16.6	11.2	10.2	2.69
High flow system	1.09	5.7	81.6	18.4	26.0	16.3	15.3	6.85
		8.7	77.1	22.9	14.5	9.4	—	3.94
		11.7	77.1	22.9	11.2	7.2	—	3.03
		14.2	78.6	21.4	15.2	9.7	10.2	4.08
	1.55	5.7	86.9	13.1	26.3	15.9	—	9.51
		8.7	86.3	13.7	23.8	14.5	—	8.7
		11.7	86.9	13.1	26.3	15.9	—	9.54
		14.2	86.7	13.3	23.4	14.1	15.2	8.48
	2.33	5.7	87.4	12.6	25.9	15.5	17.8	13.95
		8.7	85.4	12.7	25.6	15.0	—	13.5
		11.7	87.2	12.8	22.8	13.7	—	12.3
		14.2	87.5	12.5	21.0	12.6	—	11.3

Table II. Comparison of composition measured by SEM/EDAX and chemical analysis

Sample	Method: Chemical analysis (a/o) Ni	Chemical analysis (a/o) P	SEM/EDAX (a/o) Ni	SEM/EDAX (a/o) P
0.31 A/cm^2, 5.7 m/s	75.1	24.9	71.3	28.7
1.09 A/cm^2, 5.7 m/s	82.6	17.4	81.6	18.4
1.55 A/cm^2, 5.7 m/s	87.9	12.1	86.9	13.1
2.33 A/cm^2, 5.7 m/s	88.5	11.5	87.4	12.6

and

$$H_2PO_2^- + e^- \rightarrow P(s) + 2\ OH^- \qquad [4]$$

For the thickness calculation, the alloy was considered to contain only nickel and phosphorus and its density was calculated by the following equation

$$\frac{1}{\rho_{alloy}} = \frac{\text{w/o of Ni}}{100 \times \rho_{Ni}} + \frac{\text{w/o of } P}{100 \times \rho_p} \qquad [5]$$

where w/o is weight percent. These calculated thicknesses were found to agree within 15% with measured values (Table I).

Figure 2 shows the alloy composition as a function of flow rate. Electrolyte flow exerts considerable influence on an electrodepositing system which is operating in the laminar regime. In general, the mass-transfer limitation is more severe at higher current density, and a rapidly flowing electrolyte is commonly used to alleviate this problem. However, as this flow rate is increased into the turbulent regime, its influence wanes. In this work, the electrolyte flow rate was varied from 5.7 to 14.2 m/s, corresponding to a Reynolds number range of 1.8×10^4 to 4.6×10^4, well above the laminar/turbulent transition point for a rectangular channel. As seen in Fig. 2, there is no strong influence of flow rate on alloy composition in this turbulent regime. Even the lowest flow rate (5.7 m/s) is sufficiently high to induce mixing of the fluid at the electrode surface.

The alloy composition, on the other hand, varies with current density, as shown in Fig. 3 which includes results from the electroless bath and the conventional plating process. Brenner (19) and Ratzker (9) have reached this conclusion previously. In our work, the phosphorus content ranged from 28.7 a/o at 0.31 A/cm^2 to 12.5 a/o at 2.33 A/cm^2. A difference for the high flow deposition is that a coherent high phosphorus alloy film can be prepared at significantly higher current density than can be achieved with tank plating. For example, Ratzker (9) used the conventional plating process to produce a sample with 11 a/o phosphorus at a current density of 0.62 A/cm^2, whereas the same current density can yield an alloy with 28.3 a/o phosphorus in this work (Fig. 3). With a rapidly flowing fluid, the boundary layer near the surface becomes very thin and the transport of ions through this layer is greatly enhanced. In contrast, only low current density can be used in the conventional plating process due to mass-transfer

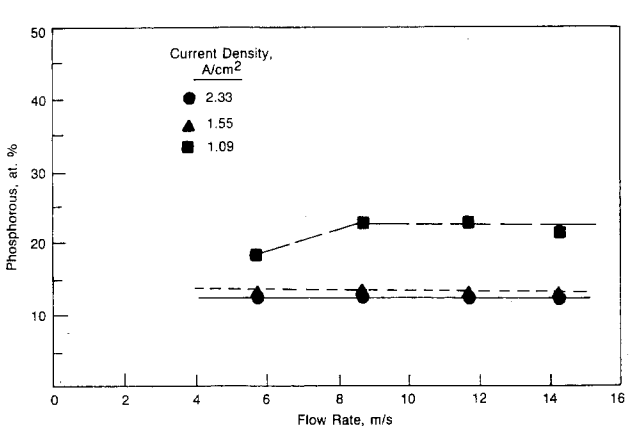

Fig. 2. Effect of flow rate on phosphorus content

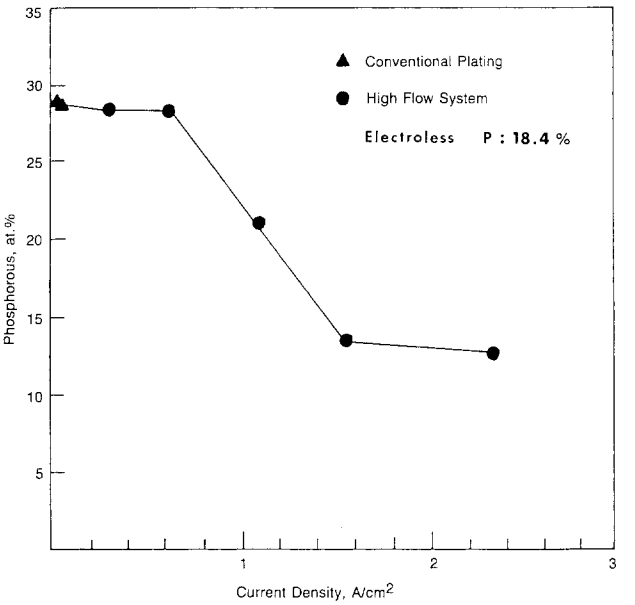

Fig. 3. Effect of current density of phosphorus content

limitation of the reacting species. Another advantage of the high flow system is the significantly higher deposition rate (μm/min), as shown in Table I.

The plating current efficiencies in this work (Table I) are generally below 30%. Figure 4 shows the effect of current density on current efficiency at different flow rates. The curves suggest a trend of increasing current efficiency with current density until the latter reaches 1.55 A/cm^2 after which the current efficiency decreases. This trend is in agreement with the work by LaBoda (18) on high speed nickel plating. A limiting current situation exists around 1.55 A/cm^2 where the surface concentration of the reacting species reaches zero, and any further increase in current density only enhances the evolution of hydrogen gas. A higher flow rate also increases the transport of hydrogen ions to the surface and gives a lower current efficiency.

Structure and microstructure of As-plated deposits.—All deposits appeared bright and metallic. A typical example is shown in the Fig. 5 photomicrograph, the result of depositing at 2.33 A/cm^2 current density and 11.7 m/s linear flow velocity. The line pattern follows the direction of flow, but more work is needed to identify its cause.

Diffractograms of alloys with high phosphorus content (>14 a/o) exhibit rounded broad maxima (Fig. 6a, b) with

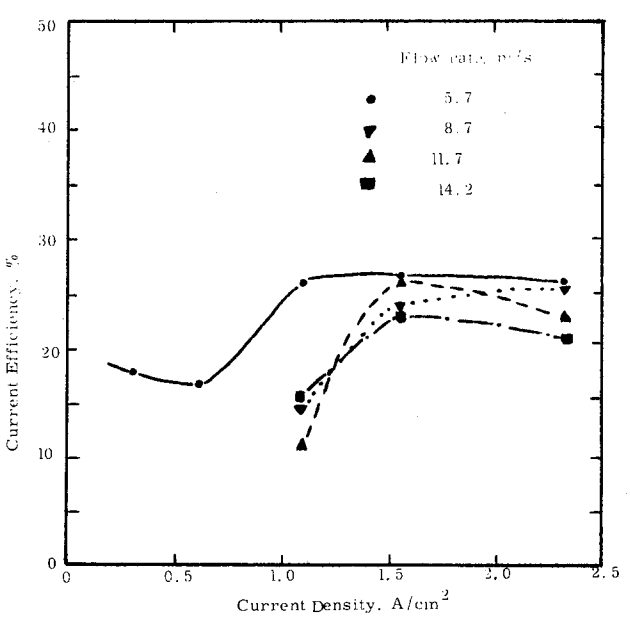

Fig. 4. Effect of current density on current efficiency at different flow rates.

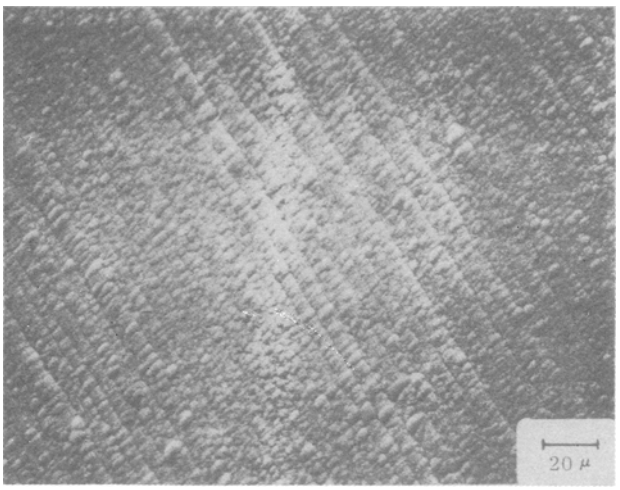

Fig. 5. SEM picture of NiP deposit (2.33 A/cm^2, 11.7 m/s)

widths which correspond to a crystallite size of 1 nm, suggesting that these alloys are amorphous. As the phosphorus concentration decreases, the diffraction peak sharpens (Fig. 6c, d), indicating that a transition from amorphous to microcrystalline has occurred. The sharp peaks in Fig. 6d are those of the copper substrate. The peak width for an alloy with a phosphorus content of 18.4 a/o (Fig. 6c) corresponds to a crystallite size of 2 nm.

A further decrease of phosphorus concentration to 12 a/o leads to a further decrease in diffraction peak width and a dramatic increase in peak intensity (Fig. 6e). This diffraction pattern is interesting in that it exhibits only one strong peak, corresponding to the fcc (111) d-spacing. Close examination reveals that weak (220) and (311) peaks are also present. This suggests that there is some preferred crystal orientation texture in this sample. In order to further investigate texture, x-ray diffraction in symmetric reflecting geometry was performed. In this diffraction geometry, the crystallographic planes which diffract are parallel to the sample surface. Only two peaks were observed, the (111) and (222), indicating a preference for the close-packed planes to lie in the plane of the sample. Rocking curve measurements confirmed this conclusion; however, the rocking curve is relatively broad (>15°). In addition, analysis of the peak widths indicates that there is substantial inhomogeneous strain (1.7%) in this sample. The fcc structure of the deposit is highly strained by the phosphorus content and the high flow growth conditions, and growth in the (111) direction is thus preferred, as suggested by Bestgen (10).

Phase transformation of alloys.—Phase transformation of the metastable nickel-phosphorus deposits were characterized by the combination of calorimetry and x-ray diffractometry. The crystallization of amorphous Ni-P alloys has been known to proceed through several metastable phases before reaching the final equilibrium phases (14, 20). These intermediate phases can be quite different in structure, depending on the phosphorus content.

In this work, Ni-P deposits prepared under high current density and high flow conditions were examined for their phase transformation during heat-treatment. From the DSC and x-ray results, the transformation process of electrodeposited alloys can be grouped into three categories: high phosphorus (28-29 a/o), low phosphorus (12-14 a/o) and medium phosphorus (18-23 a/o). The transformation behavior of electroless Ni-P alloys is also different from that of their electrodeposited counterparts.

High-phosphorus alloys (28-29 a/o).—An alloy with a high phosphorus content of about 28-29 a/o was prepared either in the conventional plating tank (0.022 and 0.044 A/cm^2) or in the high flow process (0.31 and 0.62 A/cm^2). As-plated, these alloys are amorphous with a broad peak around the Ni (111) orientation. When heated, the samples show a DSC trace containing three (Fig. 7a) or two (Fig. 7b) peaks, depending on current density. For samples produced in the conventional tank (Fig. 7a), the first small peak at 315°C represents the separation of fine nickel particles from the amorphous matrix. This peak was not observed in the high flow samples (Fig. 7b).

At a higher temperature of about 360°-370°C, all samples exhibit a sharp peak, signaling the start of a significant phase transformation. X-ray diffractograms (Fig. 8) were taken for samples heat-treated to 450°C to identify the possible phases. No elemental Ni peak was found in the pattern, and a computer search (21) recognized only the Ni_3P phase. However, three of the major peaks (marked * in Fig. 8) cannot be indexed with a high confidence level, but they can be indexed to either Ni_5P_2, $Ni_{12}P_5$, or Ni_2P. This unknown phase, Ni_xP_y, has been observed by other investigators (12, 15-17), and Pittermann and Ripper (14) postulated $Ni_{12}P_5$ (29.4 a/o P) as its possible indentity. Without

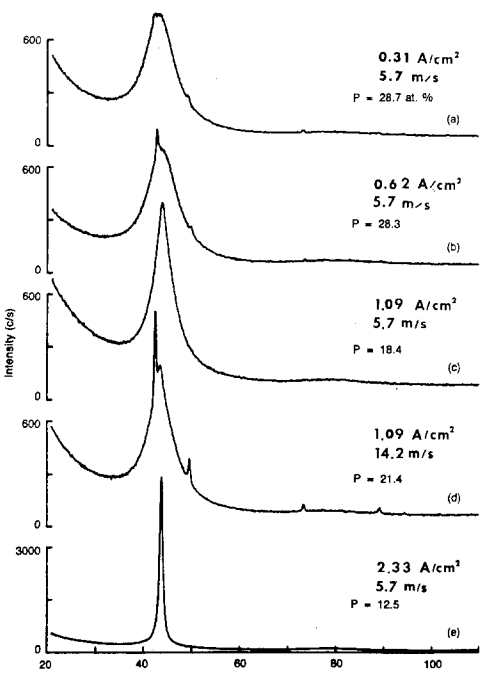

Fig. 6. X-ray diffraction of as-plated deposits with different phosphorus content.

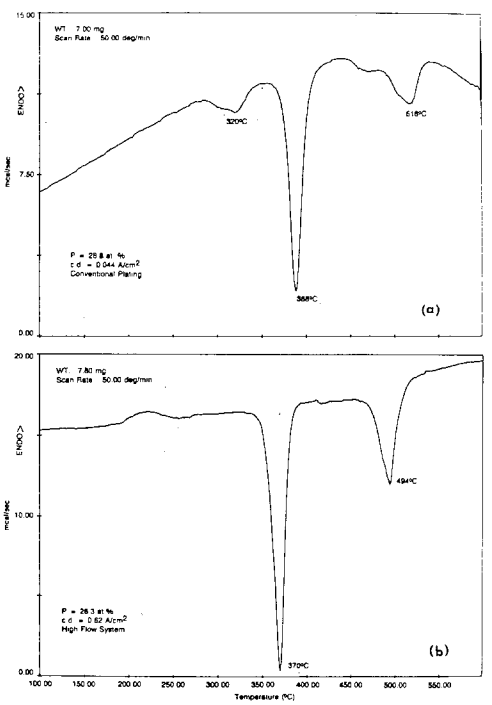

Fig. 7. DSC traces of high phosphorus (28-29 a/o) deposits: (a) conventional plating, (b) high flow rate system (5.7 m/s).

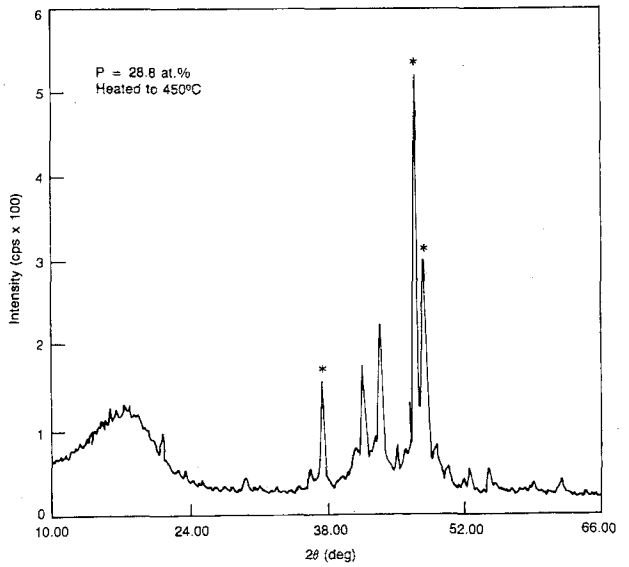

Fig. 8. X-ray diffraction of the heat-treated (to 450°C) high phosphorous deposit prepared at 0.44 A/cm^2 with the conventional plating process.

any definite identification, we will refer to it as Ni_xP_y. It is stable up to at least 450°C.

With further heating, another small broad peak appears at 500°-520°C. The x-ray pattern taken at 600°C (Fig. 9) can be indexed to a mixture of Ni and Ni_3P. The complete phase transformation can thus be represented by two steps, first, the crystallization of the amorphous Ni-P to an intermediate Ni_xP_y phase.

$$\text{Ni-P(alloy)} \rightarrow Ni_xP_y \qquad [6]$$

Ni_xP_y is metastable and decomposes on further heating (500°C)

$$Ni_xP_y \rightarrow Ni_3P + Ni \qquad [7]$$

Low phosphorus alloys (12-14 a/o).—Deposits prepared at 1.55 and 2.33 A/cm^2 have 12-14 a/o P and are crystalline as plated (Fig. 6e). Differential scanning calorimeter measurements (Fig. 10) show only one sharp peak at 420°-430°C. X-ray diffraction results at 600°C can be indexed to a mixture of Ni and Ni_3P. The supersaturated alloy thus crystallizes through the following path

$$\text{Ni-P(alloy)} \rightarrow \text{Ni (fcc)} + Ni_3P \qquad [8]$$

A small peak precedes the sharp crystallization peak in the DSC isotherm, and is due to the precipitation of fine Ni particles from the solid solution.

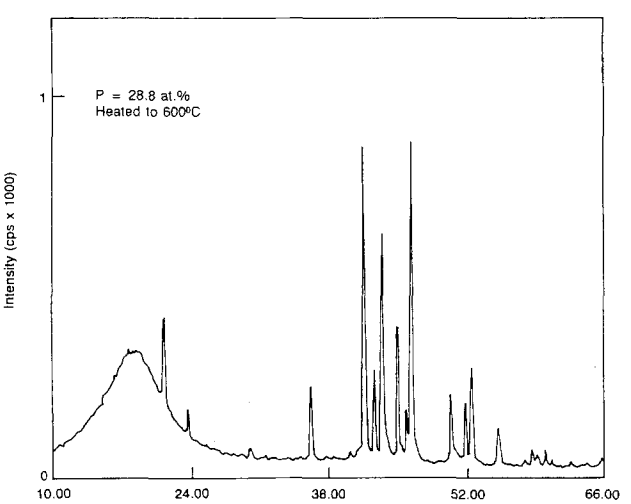

Fig. 9. X-ray diffraction of high phosphorus deposit (same preparation condition as in Fig. 8) heat-treated to 600°C.

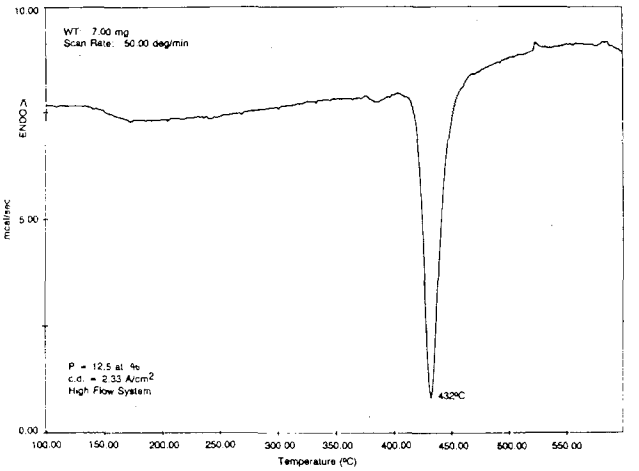

Fig. 10. DSC trace of low phosphorus deposit prepared with the high flow system (5.7 m/s).

Medium phosphorus alloys (18-23 a/o).—In between the high (amorphous) and low (crystalline) phosphorus alloys lie the alloys with intermediate phosphorus content. The transition from amorphous to crystalline structure occurs at the current density of 1.09 A/cm^2 which gives a phosphorus content of 18-23 a/o. At these transition stages, it is likely that both crystalline and amorphous phases exist in the deposit, and the two-phase transformation processes mentioned above will occur simultaneously when the sample is heated.

Figures 11a and b show the DSC traces for deposits with 18.4 and 21.4 a/o P, respectively. They each have three exothermal peaks, with the first two appearing close to each other in the temperature range of 370°-410°C. X-ray diffraction patterns at 450°C for both samples (Fig. 12) clearly indicate that Ni(fcc) is the major constituent, with a minor amount of both Ni_3P and the intermediate Ni_xP_y phases. The lower temperature peak (383° and 375°C) represents the transformation of crystalline Ni-P to Ni and Ni_3P, as given by Eq. [8]. At higher temperatures (408° and 386°C), the amorphous part of the deposit transforms to the intermediate phase, Ni_xP_y, according to Eq. [6]. Finally, at further heating (488° and 478°C), the intermediate Ni_xP_y phase

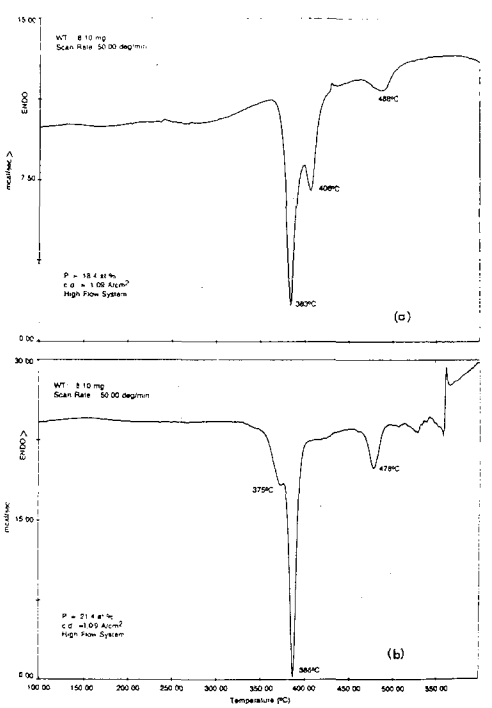

Fig. 11. DSC traces of medium phosphorus deposits prepared at 1.09 A/cm^2 with the high flow system. (a) P, 18.4 c/o, 5.7 m/s; (b) P, 21.4 a/o, 14.2 m/s.

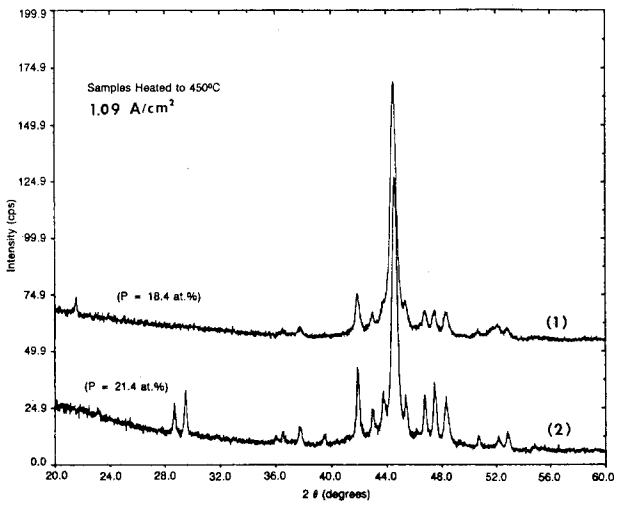

Fig. 12. X-ray diffraction of medium phosphorus deposits heat-treated to 450°C. (1)P, 18.4 a/o, 5.7 m/s; (2) P, 21.4 a/o, 14.2 m/s.

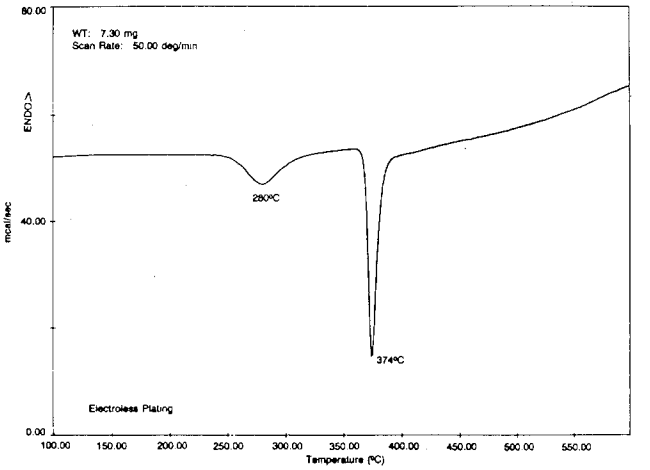

Fig. 13. DSC trace of electroless NiP alloys

decomposes to crystalline Ni and Ni_3P (Eq. [7]). X-ray diffraction patterns at 600°C show only Ni and Ni_3P.

Alloys prepared by chemical deposition (electroless) in this work have about 18 a/o P and are amorphous as-plated. During heating (Fig. 13), a phase separation occurs at about 280°C when fine Ni particles are precipitated out from the amorphous matrix. At 375°C, crystallization starts by forming the final mixture of Ni and Ni_3P, as verified by x-ray diffraction patterns. This phase transformation is different from those of electrodeposited samples at the same phosphorus content and probably is the result of preparation technique (16).

Conclusions

With a controlled high flow system, amorphous nickel phosphorus alloys can be prepared by electrodeposition at high current densities inaccessible to conventional tank plating process. A deposit with 28 a/o phosphorus can be produced at a flow rate of 5.7 m/s, ten times faster than with conventional tank plating.

The as-plated samples are supersaturated solid solutions of phosphorus in nickel which are amorphous or highly microcrystalline at a phosphorus content greater than 14 a/o. At lower phosphorus concentration the deposits become more crystalline with the (111) plane being the direction of preferred growth. When heated, the deposits approach the final equilibrium phases by two different routes. For low phosphorus samples (<14 a/o), the nickel phosphide matrix decomposes directly to a mixture of Ni and Ni_3P, the fraction of which grows in size with further heating. Deposits with higher phosphorus content, however, go through the following phase transformation.

$$\text{Ni-P} \xrightarrow{380°\text{-}400°\text{C}} \text{Ni}_x\text{P}_y \xrightarrow{470°\text{-}500°\text{C}} \text{Ni} + \text{Ni}_3\text{P}$$

Ni_xP_y is an intermediate phase whose x-ray diffraction patterns cannot be indexed, and its stability increases with increasing phosphorus content. It eventually decomposes to Ni and Ni_3P at higher temperatures.

Acknowledgment

The authors would like to thank Jack Johnson of the Analytical Chemistry Department for conducting the x-ray diffraction measurements on the samples.

Manuscript submitted July 13, 1987; revised manuscript received Aug. 28, 1987.

General Motors Research Laboratories assisted in meeting the publication costs of this article.

REFERENCES

1. U. Ma and D. T. Gawne, *Trans. Inst. Met. Finish.*, **63**(2), 64 (1985).
2. M. Fernandez, J. M. Martinez-Duart, and J. M. Albella, *Electrochim. Acta*, **31**(1), 55 (1986).
3. S. Yoshida, H. Yamashita, T. Funabiki, and T. Yonezawa, *J. Chem. Soc., Faraday Trans.*, **80**, 1435 (1984).
4. S. Yoshida, H. Yamashita, T. Funabiki, and T. Yonezawa, *J. Chem. Soc., Faraday Trans.*, **80**, 2485 (1984).
5. D. A. Luke, *Trans. Inst. Met. Finish.*, **64**(3), 99 (1986).
6. A. Brenner and G. E. Riddell, *J. Res. Nat. Bur. Stand.*, **39**, 385 (1947).
7. A. Mayer, K. Staudhammer, and K. Johnson, *Plat. Surf. Finish.*, 76, (Nov. 1985).
8. C. Rajagopal, D. Mukherjee, and K. S. Rajagopalan, *Met. Finish.*, 59, (Jan. 1984).
9. M. Ratzker, D. Lashmore, and K. W. Pratt, *Plat. Surf. Finish.*, 74, (Sept. 1986).
10. H. Bestgen, in "Rapidly Quenched Metals," S. Steeb and H. Warlimont, Editors, p. 443, Elsevier Pub. Co., Amsterdam (1985).
11. M. Hansen, "Constitution of Binary Alloys," McGraw-Hill, Inc., New York (1958).
12. E. Vafaeii-Makhsoos, E. L. Thomas, and L. E. Toth, *Metall. Trans.*, **9A**, 1449 (1978).
13. K. Musaka and M. Maeda, *Phys. Status Solidi*, **57**, K93 (1980).
14. U. Pittermann and S. Ripper, *ibid.*, **93A**, 131 (1986).
15. W. Liu, G. Li, and G. Lu, *Trans. Met. Heat Treat.*, **2**, 57 (1981).
16. B. G. Bagley and D. Turnbull, *J. Appl. Phys.*, **39**, 5681 (1968).
17. J. P. Randin and H. E. Hintermann, *This Journal*, **115**, 480 (1968).
18. J. P. Hoare, B. J. Howie, and M. A. LaBoda, *Plat. Surf. Finish.*, **73**(9), 62 (1986).
19. A. Brenner, "Electrodeposition of Alloys," Vol. 2, p. 466, Academic Press, New York, (1963).
20. K. Masui, S. Maruno, and T. Yamada, *J. Jpn. Inst. Metals*, **41**, 1130 (1977); **44**, 124 (1980).
21. Joint Committee on Powder Diffraction Standards, Index to the Powder Diffraction File (1986).
22. M. Hansen, "Constitution of Binary Alloys," 2nd ed., p. 1027, McGraw-Hill, Inc., New York (1958).